

2006

Western Caribbean Sea Surface Temperatures During the Late Quaternary


Matthew W. Schmidt

Old Dominion University, mwschmid@odu.edu

Maryline J. Vautravers

Howard J. Spero

Follow this and additional works at: https://digitalcommons.odu.edu/oeas_fac_pubs

 Part of the [Geochemistry Commons](#), [Geophysics and Seismology Commons](#), [Oceanography Commons](#), and the [Paleontology Commons](#)

Repository Citation

Schmidt, Matthew W.; Vautravers, Maryline J.; and Spero, Howard J., "Western Caribbean Sea Surface Temperatures During the Late Quaternary" (2006). *OEAS Faculty Publications*. 219.
https://digitalcommons.odu.edu/oeas_fac_pubs/219

Original Publication Citation

Schmidt, M. W., Vautravers, M. J., & Spero, H. J. (2006). Western Caribbean sea surface temperatures during the late Quaternary. *Geochemistry, Geophysics, Geosystems*, 7(2), Q02P10. doi:10.1029/2005GC000957



Western Caribbean sea surface temperatures during the late Quaternary

Matthew W. Schmidt

Department of Geology, University of California Davis, One Shields Avenue, Davis, California 95616, USA

*Now at School of Earth and Atmospheric Sciences, Georgia Institute of Technology, Atlanta, Georgia 30332-0340, USA
(mschmidt@eas.gatech.edu)*

Maryline J. Vautravers

Godwin Laboratory for Palaeoclimate Research, Department of Earth Sciences, University of Cambridge, Downing Street, Cambridge CB3 3EQ, UK

Now at British Antarctic Survey, High Cross, Madingley Road, Cambridge CB3 0ET, UK (mava@bas.ac.uk)

Howard J. Spero

Department of Geology, University of California Davis, One Shields Avenue, Davis, California 95616, USA

[1] Mg/Ca ratios in the planktonic foraminifera *Globigerinoides ruber* from Colombian Basin core ODP 999A suggest that Caribbean sea surface temperatures (SSTs) were from 2.1 to 2.7°C colder than the present during the last three glacial maximums. In comparison, faunal derived SSTs (SIMMAX method) show that August SSTs in the Caribbean varied <2°C over the past 360 kyr, whereas February SSTs varied between 21.0°C and 26.5°C. Changes in the Mg/Ca-SST record contain a strong 23 kyr periodicity, suggesting the Mg/Ca-SST record reflects a warm season weighted SST average rather than an annual mean SST. Combining several dissolution indices, we identify brief periods of decreased carbonate preservation in our record and show that MIS 11 stands out as the most intensive dissolution cycle in the Caribbean over the last 460 kyr. Comparison of Caribbean SST change with a similar estimate of tropical SST variability in the western Pacific over the past 360 kyr reveals shifts in the east-west tropical SST gradient that are coeval with glacial-interglacial climate change and consistent both with a southward migration of the glacial ITCZ and with a glacial El Niño-like mode of tropical circulation.

Components: 10,961 words, 8 figures, 3 tables.

Keywords: Caribbean Sea; *G. ruber*; ITCZ; Mg/Ca thermometry; paleoclimate; tropical SST.

Index Terms: 3344 Atmospheric Processes: Paleoclimatology (0473, 4900); 4934 Paleooceanography: Insolation forcing; 4954 Paleooceanography: Sea surface temperature.

Received 2 March 2005; **Revised** 20 October 2005; **Accepted** 7 December 2005; **Published** 17 February 2006.

Schmidt, M. W., M. J. Vautravers, and H. J. Spero (2006), Western Caribbean sea surface temperatures during the late Quaternary, *Geochem. Geophys. Geosyst.*, 7, Q02P10, doi:10.1029/2005GC000957.

Theme: Development of the Foraminiferal Mg/Ca Proxy for Paleooceanography
Guest Editor: Pamela Martin

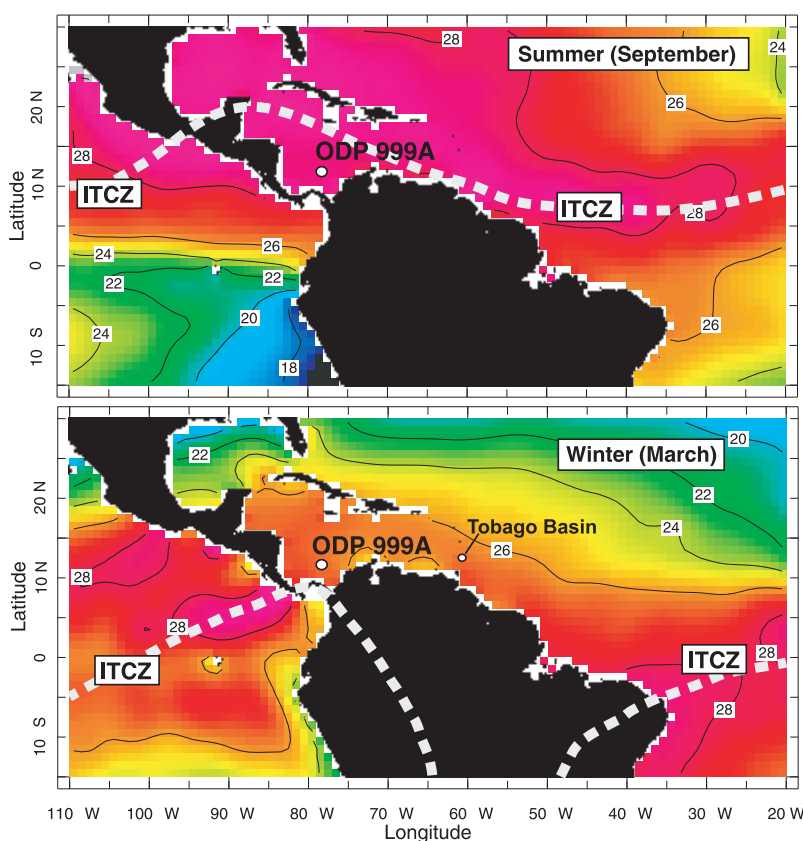


Figure 1. Average summer (September) and winter (March) SST in the western tropical Atlantic and the eastern tropical Pacific [Conkright *et al.*, 2002]. The locations of ODP 999A in the Colombian Basin and the Tobago Basin are also indicated. The dashed white line represents the seasonal location of the ITCZ.

1. Introduction

[2] Numerous ocean-atmosphere model results point to the tropics as playing a major role in forcing global climate and past climate change [Bush and Philander, 1998; Cane and Clement, 1999; Cane, 1998; Clement and Cane, 1999; Clement *et al.*, 1999; Kukla *et al.*, 2002]. These studies suggest that changes in the seasonal distribution of insolation due to orbital configuration variability may influence global climate through their influence on El Niño/Southern Oscillation (ENSO). The tropics are also a major source of water vapor, one of the atmosphere's main greenhouse gases. Atmospheric moisture content is strongly influenced by sea surface temperature (SST), so tropical SST variability should influence global climate on glacial-interglacial timescales [Pierrehumbert, 1995]. Quantifying the magnitude and timing of SST change across the tropics therefore is an important step toward evaluation of hypotheses calling for the tropics as a driver of past climate change.

[3] The Caribbean Sea plays an important role in the transport of heat and water mass to the high latitude north Atlantic because tropical equatorial surface currents flow through the Caribbean before forming the strong western Atlantic boundary current, the Gulf Stream. The Gulf Stream carries heat and salt to the high latitude Atlantic, where water vapor escapes from surface currents and warms the northern hemisphere atmosphere [Roemmich and Wunsch, 1985]. The resulting cold, dense surface waters then sink to great depth and circulate southward, thereby maintaining North Atlantic meridional overturning circulation (MOC). During periods of reduced overturning circulation, the high latitudes cool and the tropical western and south Atlantic warm as the northward heat transport is diminished [Manabe and Stouffer, 1997; Ruhlemann *et al.*, 1999; Seidov and Maslin, 2001].

[4] To investigate the history of tropical SST change in the Atlantic basin during the late Quaternary, we present a continuous planktonic foraminiferal Mg/Ca record from the Caribbean (average

1.3 kyr sampling resolution) over the past four glacial cycles (460 kyr) and a faunal-SST reconstruction (average 2.6 kyr sampling resolution) over the past three glacial cycles (360 kyr). A number of studies have already generated continuous Pacific SST records over parts of the last several glacial cycles using Mg/Ca paleothermometry, linking SST and hydrologic changes in the tropics to both orbital- and millennial-scale high latitude climate change in both the northern and southern hemispheres [Koutavas *et al.*, 2002; Lea *et al.*, 2000; Rosenthal *et al.*, 2003; Stott *et al.*, 2002; Visser *et al.*, 2003]. In this study, (1) we present data that allow us to assess the impact of dissolution on our Mg/Ca record, (2) we demonstrate that the extended Caribbean Mg-SST record shows a strong precessional component, suggesting that the Mg/Ca-SST record reflects a warm season weighted SST average, rather than annual mean SST, and (3) we compare our new long-term Caribbean SST record with a previously published record of SST change in the western tropical Pacific to gain a more complete picture of tropical climate variability through time.

2. Study Area and ITCZ Variation

[5] Paired $\delta^{18}\text{O}$ and Mg/Ca measurements are presented from the surface dwelling foraminifera *Globigerinoides ruber* (white variety) from Ocean Drilling Program (ODP) Site 999A (12°45'N, 78°44'W; 4 cm/kyr sed. rate) located in the western Caribbean (Figure 1). Core 999A was raised from the Kogi Rise at a depth of 2,827 m, about 1000 m above the turbidite-laden floor of the Colombian Basin [Mutti, 2000]. The site is directly influenced by the warm Caribbean Current and is ideally suited to reconstruct changes in southern Caribbean surface water hydrography as demonstrated by the recent study of calcareous nannofossil populations over the same interval at Site 999A [Kameo *et al.*, 2004].

[6] The Atlantic Intertropical Convergence Zone (ITCZ) extends from the west coast of Africa to northern South America and is defined as the region where the northeast and southeast Atlantic trade winds meet, resulting in a band of atmospheric convection and high precipitation located over the warmest surface waters [Philander *et al.*, 1996]. Thus the position of the ITCZ is controlled by seasonal insolation and varies throughout the year. Under modern conditions in the tropical western Atlantic, the ITCZ extends as far north as the upper Amazon and Orinoco basins and to the

Costa Rica/Nicaragua border during the boreal summer and as far south as the Amazon Basin and southern Colombia and Ecuador during boreal winter [Poveda *et al.*, 2006] (Figure 1). The meridional migration of ITCZ therefore exerts a strong control on the annual hydrologic cycle of Central and South America and on the Caribbean Sea. As a result, climate in the modern Colombian Basin is characterized by two distinct seasons: a warm, wet season in late summer and early fall when the ITCZ is located farthest to the north, and a cool, dry season during boreal winter when the ITCZ migrates south [Stidd, 1967]. The modern annual SST in the Colombian Basin averages 27.7°C, attaining a minimum of 26.6°C in March and a maximum of 28.5°C in September and October [Conkright *et al.*, 2002] (Figure 1).

[7] Several studies have linked North Atlantic cooling to a southward migration in the mean position of the Atlantic ITCZ on centennial, millennial, and orbital timescales [Black *et al.*, 1999; Hughen *et al.*, 1996; Lin *et al.*, 1997; Peterson and Haug, 2006; Peterson *et al.*, 2000; Schmidt *et al.*, 2004; Yarincik *et al.*, 2000]. According to these studies, cool periods in the North Atlantic such as the Last Glacial Maximum (LGM), the Younger Dryas (YD) and the Little Ice Age are associated with a southward shift in the ITCZ, resulting in a dryer Circum-Caribbean climate. Modeling studies also suggest a southward displacement of the ITCZ associated with periods of reduced North Atlantic MOC and northern hemisphere cooling [Schiller *et al.*, 1997; Vellinga and Wood, 2002], resulting in reduced rainfall in northern South America coupled with a wetter tropical South American climate [Peterson and Haug, 2006].

3. Materials and Methods

[8] Sediment from each core interval was disaggregated in ultra-pure water, wet sieved over a 63 μm mesh and dried at room temperature. To minimize intraspecific variation in shell geochemistry at each core interval, specimens of *G. ruber* (white variety) were only collected from the 250–350 μm size fraction [Lea *et al.*, 2000; Spero *et al.*, 2003]. Statistical analyses have demonstrated that it is necessary to analyze a large number of shells from each interval to be confident that the oxygen isotope value obtained off the mass spectrometer is a good approximation of the population mean for a given period of time [Schiffelbein and Hills, 1984; Spero, 1992]. Therefore we used at least 25 shells

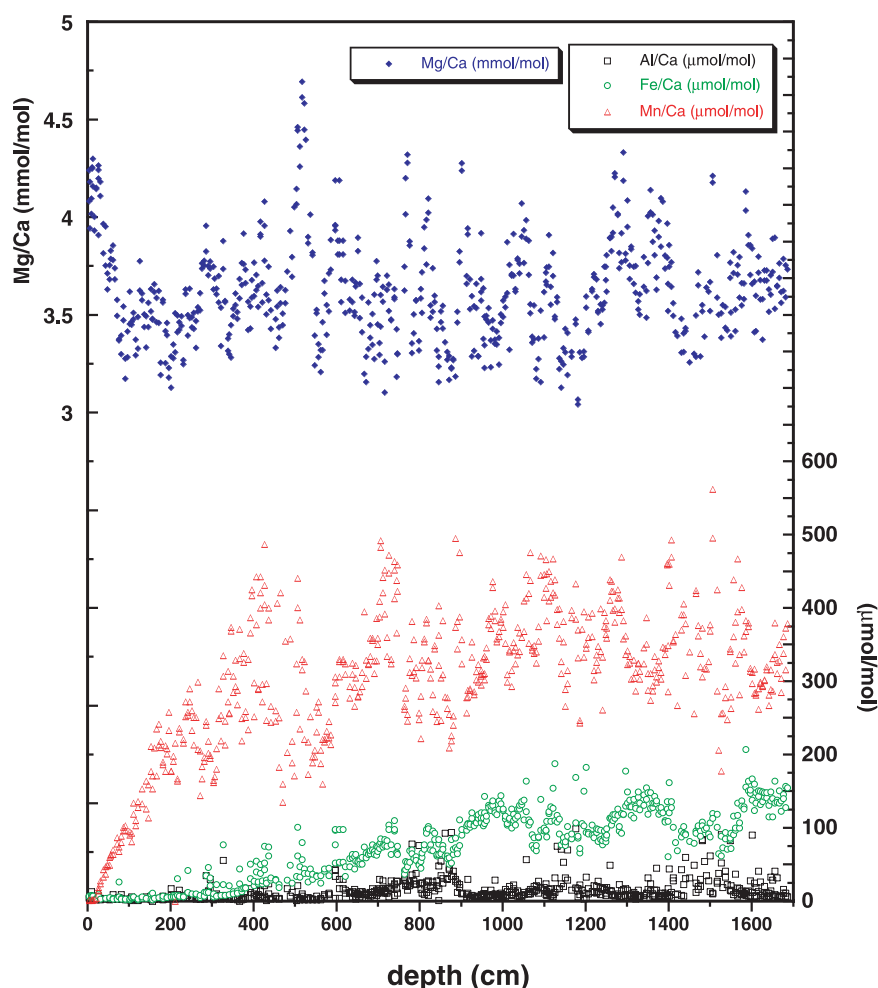


Figure 2. Measured Mg/Ca ratios (blue diamonds), Mn/Ca (red triangles), Fe/Ca (green circles), and Al/Ca (black squares) in the planktonic foraminifer *G. ruber* (white) (250–350 μm size fraction) from ODP 999A versus depth.

per stable isotope analysis for all down-core measurements. Samples for stable isotopes were sonicated in methanol for 3–8 seconds, roasted in vacuo at 375°C for 30 minutes, and analyzed at UC Davis on a Micromass Optima IRMS using an Isocarb common acid bath autocarbonate system at 90°C and calibrated using NBS 19 and UCD-SM92.

[9] Sea surface temperatures were determined using Mg/Ca ratios measured on different shells but from the same population and size fraction of *G. ruber* (white variety) specimens that were used for the stable isotope analyses. Approximately 600 μg of shell/sample (50–60 shells/interval) was cleaned for trace and minor element analysis without the DTPA step [Lea et al., 2000; Mashiotto et al., 1999]. Samples underwent a multistep process consisting of initial rinses in ultra-pure water, followed by treatments with hot reducing and

oxidizing solutions, transfers into new acid-leached micro-centrifuge vials, and finally leaches with a dilute ultra-pure acid solution. All clean work was conducted in laminar flow benches under trace metal clean conditions. Samples were then dissolved and analyzed on a Finnigan Element-2 ICP-MS at UC Santa Barbara using the established procedures described by Lea and Martin [1996], Mashiotto et al. [1999] and Lea et al. [2000]. *G. ruber* samples from every interval were divided in half and each replicate was analyzed for minor and trace elements (Figure 2). Thus each reported Mg/Ca ratio is the average of at least two analyses (Figure 3). A full suite of trace and minor element measurements were made on each sample including, Ca, Mg, Sr, Na, Ba, La, Ce, Nd, U, Al, Mn, and Fe.

[10] Below a depth of 1.5 m in the core, Mn/Ca ratios in ODP 999A exceed 200 $\mu\text{mol/mol}$ and

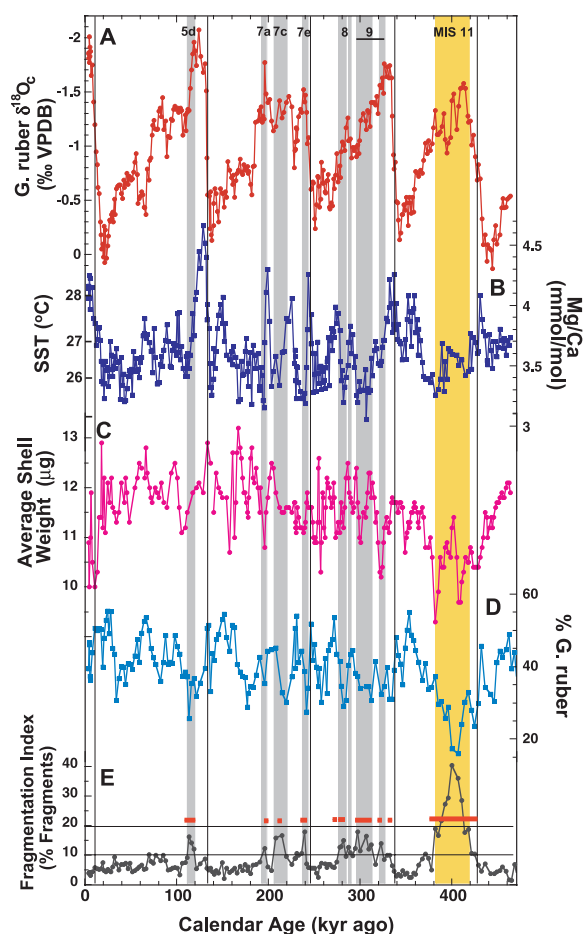


Figure 3. (a) $\delta^{18}\text{O}_e$ and (b) Mg/Ca ratios in *G. ruber* (white) from ODP 999A over the past 465 kyr. (c) Average shell weight for each interval. (d) Abundance of *G. ruber* (pink and white) in each faunal assemblage (% *G. ruber*). (e) Black line is the fragmentation index (% fragments). The red bars highlight intervals where the foraminiferal hardness index was <2 , indicating the *G. ruber* shells were notably soft as a result of partial dissolution. The gray bars indicate intervals where the fragmentation index is between 10 and 20%, and the yellow bar indicates the interval where the fragmentation index is $>20\%$. Numbered marine isotope stages at the top of the plot indicate intervals where the Mg/Ca ratios may have been reduced due to dissolution. Vertical black lines indicate glacial termination events I–V.

appear to oscillate on glacial-interglacial timescales (Figure 2). Although there is not a statistically significant relationship between Mg/Ca and Mn/Ca in the overall record, discrete intervals do show a statistically significant relationship. Because living planktonic foraminifera only incorporate a trace amount of Mn into their shells, most of the measured Mn in our cleaned foraminiferal calcite must be due to diagenetic overprinting, possibly

the result of a mixed $(\text{Mn}_x, \text{Mg}_y)\text{CaCO}_3$ mineral phase that precipitates on shell surfaces under anoxic conditions in the sediment [Pena *et al.*, 2004, 2005]. The molar ratio of Mn:Mg in authigenic Mn-carbonates from the Panama Basin is $\sim 10:1$ [Pedersen and Price, 1982; Pena *et al.*, 2005]. Assuming a similar Mn:Mg ratio in the Mn-carbonate from site 999A, the Mg/Ca contribution from these diagenetic overgrowths would be <0.05 $\mu\text{mol/mol}$, or $<1.4\%$ of the average Mg/Ca ratio in our record (Figure 2). A $\sim 9\%$ change in Mg/Ca equates to a 1°C SST change based on Mg/Ca-SST calibrations [Dekens *et al.*, 2002], so at the levels measured in our record, this diagenetic source of Mg does not significantly contribute to the primary Mg/Ca signal used for SST reconstructions.

[11] Mg/Ca ratios are converted to SST utilizing the depth-corrected *G. ruber* Mg/Ca-SST calibration of Dekens *et al.* [2002] for the tropical Atlantic:

$$\text{Mg/Ca} = 0.38 \exp 0.09[\text{SST} - 0.61(\text{water depth km})].$$

For water depth, a value of 2.8 was used for ODP 999A.

[12] Elemental ratios of Fe/Ca and Al/Ca are used to monitor cleaning efficacy (Figure 2). Analyses with anomalously high Fe/Ca or Al/Ca ratios were rerun or rejected. In addition, analyses with a post-cleaning percent recovery of $<15\%$ had anomalously low Mg/Ca ratios so these samples were either rerun or rejected. Although Fe/Ca ratios gradually increased with depth in the core (but rarely exceeded $175 \mu\text{mol/mol}$), Al/Ca ratios remained uniformly low (Figure 2), and typically less than $40 \mu\text{mol/mol}$, indicating that Mg contamination associated with detrital sediment in cleaned samples was not an issue. Mg/Ca did not correlate with Fe/Ca or Al/Ca, indicating that the mineral phases containing these metals in the cleaned samples did not affect Mg/Ca ratios in the foraminiferal calcite. All geochemical data are posted on the Web and are available at <http://www.ngdc.noaa.gov/paleo/paleo.html>.

4. Error Analysis

[13] Analytical precision for the $\delta^{18}\text{O}_e$ measurements is better than $\pm 0.06\text{‰}$ (1σ). Mg/Ca analytical reproducibility, determined by the analysis of consistency standards matched in concentration and Mg/Ca ratio to dissolved foraminifera solutions is estimated at $\pm 0.7\%$ (1σ). The pooled

Table 1. AMS ^{14}C and Calendar Ages

Core	Section	Depth, cm	CAMS #	$\Delta^{14}\text{C}$	^{14}C AMS Age	Error, years	Calendar Age, kyr B.P.
ODP 999A	1H-01	0–2	80931	–363.1	3,625	± 35	3,522
ODP 999A	1H-01	20–22	80932	–489.6	5,400	± 35	5,745
ODP 999A	1H-01	42–44	80933	–700.9	9,685	± 35	10,318
ODP 999A	1H-01	47–49	94699	–731.0	10,540	± 35	11,647
ODP 999A	1H-01	65–67	94700	–828.1	14,145	± 40	16,381
ODP 999A	1H-01	95–97	94701	–902.8	18,720	± 70	21,646

standard deviation of replicate Mg/Ca analyses from ODP 999A is $\pm 1.9\%$ (1 SD, $df = 324$) based on 348 analyzed intervals. The overall precision of replicates in this study is slightly better than other tropical cores (typically $\sim 3\%$) [Lea et al., 2000, 2003], most likely reflecting the stability of the water column in the Colombian Basin during the last 460 kyr.

5. Micropaleontology Study

[14] Before the preparation for isotopic and minor/trace metal geochemistry measurements, split samples representing 1/8 of the initially sieved samples were reserved for micropaleontological analysis. Identification of planktonic foraminifera species from the $>150\text{ }\mu\text{m}$ sized fraction was performed on a representative sub-samples containing at least 300 whole specimens and usually more than 400. The taxonomy was based on Kennett and Srinivasan [1983].

[15] Faunal SST estimates for August and February were calculated using the SIMMAX method [Pflaumann et al., 1996] and a data-base of 947 core tops from the north and south Atlantic [Pflaumann et al., 2003]. Results were obtained by selecting the 5 best analogs from the database with the dissimilarity coefficient threshold set at 0.85 and without the distance weighting procedure. The statistical reliability of the faunal-SST reconstructions can be assessed by examining the number of intervals that failed to be reconstructed (6 out of 130) or by the number of intervals that cannot find 5 SIMMAX database analogues within the 0.85 similarity coefficient threshold (7 out of 130). In addition, the average value for the similarity coefficient for the reconstructed samples ($n = 124$) is 0.92, indicating that faunal-SST reconstructions for the Colombian Basin over the last 3 glacial cycles can be regarded with a good degree of confidence. However, the method was not able to find 5 analogues for 10% of the samples examined at Site

999A (13 out of 130), so there remains a need for the development of a better regional database.

[16] Faunal counts were also used to calculate the % *G. ruber* in the planktonic foraminifera community through time. The % *G. ruber* can be used to evaluate carbonate dissolution effects and to determine changes in surface and subsurface hydrological conditions.

[17] Planktonic foraminifera fragments were also counted in the same sub-samples based on the criteria that a test with less than one half of a whole test was counted as a fragment, even if the species could still be recognized. Because we do not consider that shells are fragmented into several pieces $>150\text{ }\mu\text{m}$ as proposed by Le and Shackleton

Table 2. Tie Points Used to Correlate the ODP 999A *G. ruber* $\delta^{18}\text{O}_\text{c}$ Record to SPECMAP From 22 to 465 kyr

Section	Interval, cm	Continuous Depth, cm	Age Cal B.P.
1H-02	2–5	153	32.2
1H-02	95–97	246	55.2
1H-02	140–142	291	66.4
1H-04	2–4	453	109.0
1H-04	52–54	503	121.4
1H-04	71–73	522	130.8
1H-04	130–132	581	142.9
1H-05	65–67	666	167.2
1H-06	15–17	716	181.5
2H-01	2–4	763	196.0
2H-01	25–27	786	205.0
2H-01	65–67	826	228.0
2H-01	95–97	856	231.0
2H-01	115–117	876	238.0
2H-02	25–27	936	251.0
2H-02	110–112	1021	267.0
2H-03	38–40	1099	286.0
2H-03	85–87	1146	298.0
2H-04	19–21	1230	319.0
2H-04	55–57	1266	331.0
2H-04	105–107	1316	343.0
2H-05	30–32	1391	360.0
2H-06	90–92	1601	436.0
2H-07	30–32	1691	465.0

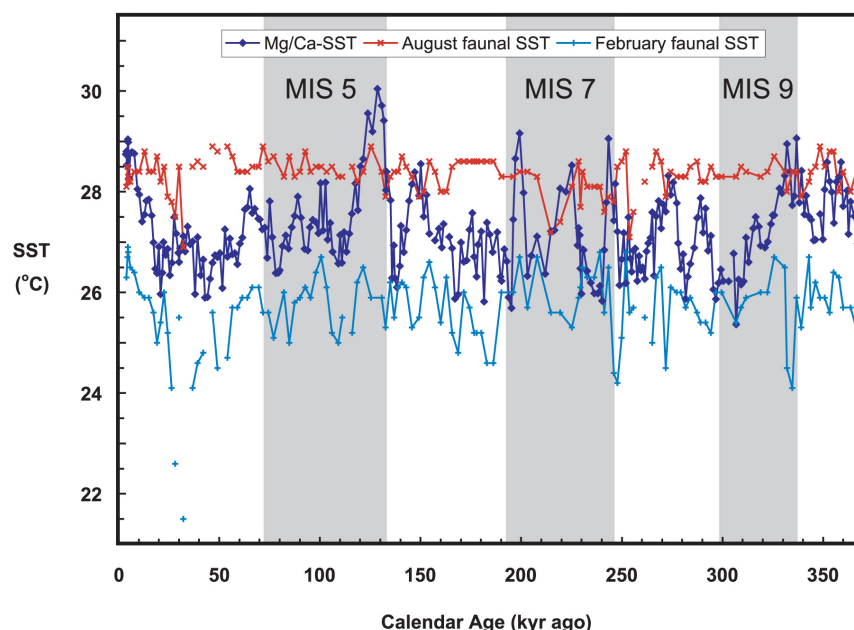


Figure 4. Caribbean SST records from Mg/Ca ratios (closed blue diamonds) and faunal SST reconstructions for August (red crosses) and February (blue pluses) calculated from the foraminiferal assemblages using SIMMAX 28 [Pflaumann et al., 1996]. Gray bars indicate interglacial marine isotope stages.

[1992], the percentage of fragments were calculated according to Howard and Prell [1994] and Berger [1970] as follows:

$$\% \text{ fpf} = 100 * (\# \text{fpf} / (\# \text{fpf} + \# \text{wfp})),$$

where # is number, fpf is fragment of planktonic foraminifera, and wfp is whole planktonic foraminifera.

6. Age Model

[18] The age model for ODP 999A from the core top to 22 kyr is based on linear interpolation between calibrated radiocarbon ages from selected depths (Table 1). All AMS ^{14}C dates were generated at the LLNL Center for Accelerator Mass Spectrometry and are based on the planktonic foraminifera *G. ruber* (white). The Calib rev. 4.3 program [Stuiver and Reimer, 1993] was used to convert ^{14}C dates into calendar age (kyr B.P.) assuming a reservoir age of 420 years [Hughen et al., 1996, 1998]. Beyond the ^{14}C -based age model (21.6 kyr B.P.), the age model is based on correlation of the *G. ruber* $\delta^{18}\text{O}_\text{c}$ record to SPECMAP [Bassinot et al., 1994b] and to estimates of sea level change from coral U-Th dates [Chappell et al., 1996] during Termination II. Table 2 lists the

tie points used to develop a SPECMAP based age model for ODP 999A.

7. Results

[19] The *G. ruber* $\delta^{18}\text{O}_\text{c}$ record from the upper 17 m of ODP 999A shows four complete glacial cycles back to MIS 12 at 460 kyr (Figure 3a). The $\delta^{18}\text{O}_\text{c}$ record across Terminations I, II and IV displays a glacial-interglacial difference of $\sim 2\%$, which falls within the range observed in other tropical Atlantic and Caribbean cores [Emiliani, 1966; Ruhlemann et al., 1999; Wolff et al., 1998]. Termination III and V display reduced glacial-interglacial differences of only 1.13‰ and 1.50‰, respectively. The Holocene and interglacials MIS 5e, 7a and 9 attain minimum values of about -2.00% , but MIS 7e and 11 have more positive $\delta^{18}\text{O}_\text{c}$ values of -1.52% and -1.58% , respectively. The LGM and MIS 12 stand out in the record with the most positive $\delta^{18}\text{O}_\text{c}$ values. Glacial maxima during MIS 6, 8, and 10 have $\delta^{18}\text{O}_\text{c}$ values close to -0.2% , but at the LGM and MIS 12, $\delta^{18}\text{O}_\text{c}$ values exceed 0‰.

[20] The Mg/Ca record yields an average Holocene SST of $28.2^\circ \pm 0.3^\circ\text{C}$ ($n = 11$) (Figure 4), in good agreement with the average modern annual SST for the Colombian Basin (27.7°C) and in even closer agreement with the regional average May–October

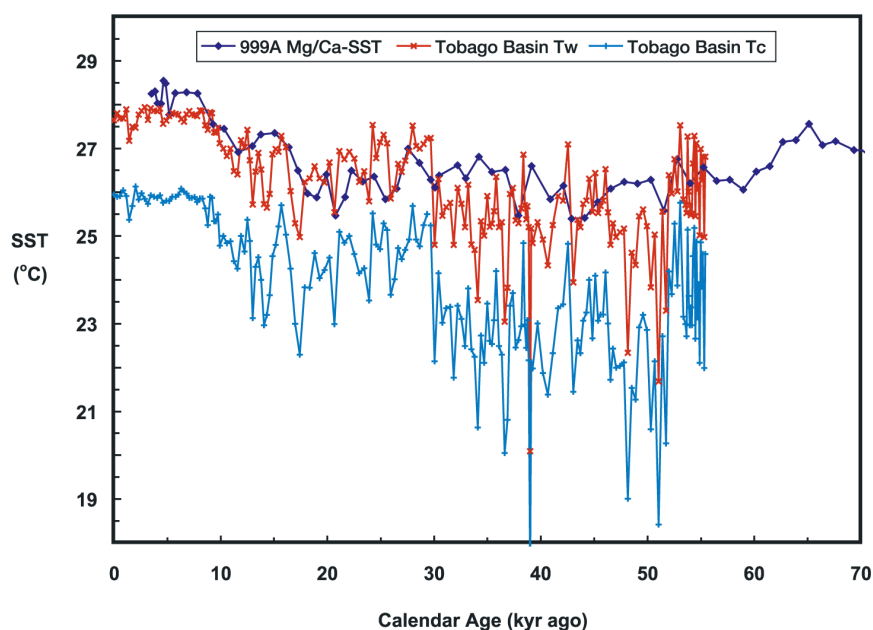


Figure 5. Comparison of the ODP 999A Mg/Ca-SST record (closed blue diamonds) over the past 55 kyr with the Tobago Basin faunal SST (modern analog technique) reconstruction for summer months (Tw) (red crosses) and for winter months (Tc) (blue pluses) [Hüls and Zahn, 2000].

average SST (28.2°C) [Conkright et al., 2002]. The core-top – LGM (18–24 kyr) Mg/Ca change equates to temperature difference of $2.1 \pm 0.4^{\circ}\text{C}$ ($n = 7$), consistent with previous estimates for the Caribbean [Hastings et al., 1998; Prell et al., 1976]. Our Mg/Ca-SST record from site 999A is similar to the Tobago Basin SST reconstruction for the summer months based on faunal census counts (modern analog technique) over the past 55 kyr [Hüls and Zahn, 2000] (Figure 5). However, the Tobago Basin SST reconstruction estimates significantly cooler winter months over the same time period, suggesting that the *G. ruber* Mg/Ca-SST record is biased toward the warmer months of the year. The Mg/Ca-SST record from ODP 999A also shows that MIS 4 (60–70 kyr) was warmer than MIS 2 and 3, with an average SST of $27.0 \pm 0.3^{\circ}\text{C}$ ($n = 9$). The long-term SST record shows that glacial-interglacial cooling is not uniform across the last four glacial termination events, with a maximum glacial-interglacial temperature difference of 3.2°C occurring at the MIS 6/5e transition (Figure 4). In addition, the Mg/Ca ratios from MIS 11 (362–423 kyr) are lower than all other interglacial intervals in the record, yielding an average SST of $26.4 \pm 0.5^{\circ}\text{C}$ ($n = 25$).

[21] The Mg/Ca-SST record from the last three glacial cycles shows the presence of apparent warming events prior to the onset of maximum

glacial conditions. These warming events (1.5 to 2°C of temperature increase) occur during MIS 6, 8 and 10 and are centered at 147, 272 and 354 kyr, respectively (Figure 4). Although smaller in magnitude, MIS 3 also shows a 1.0°C warming event at 35 kyr that is followed by a decrease to an average LGM SST of $26.1 \pm 0.4^{\circ}\text{C}$.

[22] The faunal derived SSTs show nominal August SST variation (less than $\pm 1^{\circ}\text{C}$), ranging between 28.5°C and 26.5°C with an average of 27.8°C . However, the pattern of SST fluctuation is not straightforward when compared to the glacial/interglacial delimitations. In fact, both the warmest and the coldest SSTs occur during glacial intervals (Figure 4). In contrast, February faunal-SST values show considerably more variability, ranging between 21.0°C and 26.2°C , with an average of 24.8°C . On the basis of an earlier faunal-SST reconstruction, Imbrie and Kipp [1971] found a similar Caribbean seasonal contrast over the same time interval. Faunal winter SST values during the MIS 3 - 2 transition are considerably colder than the two previous glacial intervals, MIS 6 and MIS 8. In contrast, the Mg/Ca-SST reconstruction shows very similar glacial temperatures during MIS 2, 6, and 8. Note that the Mg/Ca-SST reconstructions lie between the average August and February faunal-SST values during glacial intervals, but that Mg/Ca-SST values briefly exceed August faunal-SST estimates during certain

Table 3. Regression Analysis Results of Shell Weight Versus Mg/Ca Ratios in Discrete Glacial-Interglacial Intervals

	P-Value ^a
MIS 1	0.5715
MIS 2,3,4	0.4984
MIS 5	0.5090
MIS 6	0.1487
MIS 7	0.1224
MIS 8	0.5306
MIS 9	0.0719
MIS 10	0.4775
MIS 11 ^b	0.0007
MIS 12	0.9824

^a P-value <0.05 indicates a statistically significant relationship at the 95% confidence level.

^b Significant relationship.

interglacial periods (MIS 1, 5e, 7a, 7c, 7e, and 9) (Figure 4).

[23] The primary limitation with the Mg/Ca approach is shell dissolution and subsequent reduction in Mg/Ca during descent or after deposition on the seafloor [Brown and Elderfield, 1996; Dekens *et al.*, 2002; Lohmann, 1995; Rosenthal and Lohmann, 2002]. Because of the replacement of North Atlantic Deep Water by Antarctic Bottom Water during glacial times, as traced by variations in the $\delta^{13}\text{C}$ and Cd/Ca of benthic foraminifera [Boyle and Keigwin, 1987; Oppo and Lehman, 1993], the deep Atlantic below 2000 m was more corrosive during glacial intervals. Unlike the open Atlantic, the Caribbean displays a reverse preservation pattern. At tropical latitudes in the modern north Atlantic, the nutrient depleted (high $\delta^{13}\text{C}$) Upper North Atlantic Deep Water (UNADW) mixes with nutrient rich (low $\delta^{13}\text{C}$) Antarctic Intermediate Water (AAIW) and Upper Circumpolar Deep Water (UCDW) between 900–1900 m and enters the Caribbean Sea through its deepest sill (Anegada-Jungfern Passage) at depth of 1900 m [Johns *et al.*, 2002]. Therefore a mixture of both northern and southern sourced water masses forms the bottom waters of the Caribbean during interglacial periods like today. The southern sourced AAIW and UCDW have a lower $[\text{CO}_3^{2-}]$ content and are therefore more corrosive than UNADW. During glacial intervals, nutrient depleted (less corrosive) Glacial North Atlantic Intermediate Water replaced the southern sourced waters at mid-depths in the tropical north Atlantic [Oppo and Fairbanks, 1987; Oppo and Lehman, 1993] and in the Caribbean, resulting in better carbonate preservation in the glacial Caribbean. Because glacial intervals were periods of enhanced preservation in the Caribbean,

dissolution is less likely to have influenced our reconstructed glacial Mg/Ca-temperatures.

[24] In order to determine if dissolution has affected the Mg/Ca ratios in the interglacial intervals of ODP 999A, we present the results from three quantitative and one qualitative parameters that can be used as dissolution indices: shell weight, the percentage of total *G. ruber*, the percentage of fragments, and the foraminiferal hardness index (FHI) (Figures 3c, 3d, and 3e). The shell weight index [Lohmann, 1995] is predicted to decrease with increasing calcium carbonate dissolution. Therefore, if our Mg/Ca ratios were appreciably affected by dissolution, Mg/Ca ratios would covary with shell weight (Figures 3b and 3c). However, regression analyses of discrete glacial and interglacial intervals demonstrate that the only statistically significant relationship between Mg/Ca ratios and shell weights occurs during MIS 11 (Table 3), suggesting that this section of our Mg/Ca record is strongly affected by dissolution. Nevertheless, shell weight can be influenced by both pre- and post-depositional processes, so the relationship between shell weight and carbonate dissolution intensity must be used with caution [Barker and Elderfield, 2002; Bijma *et al.*, 1999; Broecker and Clark, 2001; de Villiers, 2004].

[25] Planktonic foraminiferal assemblages at the sediment interface are strongly influenced by the distribution of living planktonic foraminifera within the upper water column [Bé and Tolderlund, 1971]. Numerous experimental studies [Berger, 1967, 1970; Berger and Piper, 1972; Honjo and Erez, 1978] or studies based on depth transects [Adelseck, 1978; Bé *et al.*, 1975; Berger, 1968, 1970, 1982; Bonneau *et al.*, 1980; Coulbourn *et al.*, 1980] have established a planktonic foraminifera dissolution resistance scale [Berger, 1970]. In particular, species of the genus *Globigerinoides* are recognized as dissolution-sensitive species. Therefore the abundance of total *G. ruber* (pink and white varieties) in the total faunal assemblage (expressed as % *G. ruber*) can be used as a dissolution index because the % *G. ruber* is predicted to decrease with increasing dissolution. Use of the % *G. ruber* index as a dissolution proxy for the Caribbean was first proposed by Imbrie and Kipp [1971]. They concluded that the high % *G. ruber* occurring during interglacial periods ruled out major dissolution as a control on faunal assemblages in the Caribbean.

[26] However, ecological and biological responses to changes in the physical and chemical hydrogra-

phy of the Colombian Basin on glacial-interglacial timescales can also affect the % *G. ruber* at site 999A, resulting in a range of natural variability that is not related to dissolution. Across the interval from the LGM (18 kyr) through MIS 4 (70 kyr), a period considered to be characterized by enhanced preservation in the Caribbean (supported by increased shell weights and a low fragmentation index (Figures 3c and 3e)), the % *G. ruber* ranges from a low of 30% to a high of 55%, suggesting a large range of natural variability due to factors other than dissolution. If we assume that the low end of this natural variability in the % *G. ruber* is ~30%, the only intervals with lower *G. ruber* abundance occur at times of increased % fragmentation (>10%) at 113 kyr (MIS 5d) and 240 kyr (MIS 7e) and for a sustained period during MIS 11 from 390 to 428 kyr (Figure 3d). Therefore periods of exceptionally low *G. ruber* abundance suggest that dissolution was most intense during these isolated time intervals.

[27] On the basis of depth transect observations [Berger, 1982; Johnson *et al.*, 1977; Peterson and Prell, 1985], foraminiferal fragmentation increases as dissolution increases [Bassinot *et al.*, 1994a; Howard and Prell, 1994]. Shells are more easily broken as shell walls are thinned during dissolution [Bé *et al.*, 1975]. This proxy has proved to be a good qualitative dissolution tracer for deep-sea records (>2500 m) that experience a range of dissolution variability as a result of changing water masses at glacial-interglacial transitions [Bassinot *et al.*, 1994a; Howard and Prell, 1994; Le and Shackleton, 1992]. At a time when preservation was enhanced in the Caribbean during the last glacial cycle (MIS 2–4), the fragmentation index varied from 3 to 10% (Figure 4e), suggesting that variability below this threshold is typical for well-preserved foraminiferal calcite at site 999A. MIS 11 is the only interval in our record characterized by a fragmentation index >20% (yellow bar in Figure 3), indicating the most intense period of dissolution. Nevertheless, there are several intervals in our record with a fragmentation index between 10 and 20% (gray bars in Figure 3), which may have been affected to a lesser degree by dissolution.

[28] The relative hardness of *G. ruber* shells can also be used to determine intervals of more intense dissolution. Pooled shells are crushed between glass slides prior to cleaning for trace metal analysis. As the shells break, the ease of fragmentation was recorded on a scale of 1 to 5 with 1 being the

softest and 5 being the hardest). This foraminiferal hardness index (FHI), while qualitative, showed that those intervals with the softest shells (FHI < 2) (red bars in Figure 3e) corresponded to intervals where the fragmentation index is >10%. Because dissolution is predicted to thin shell walls and make foraminiferal calcite softer, this index confirms that parts of MIS 5d, 7a, 7c, 7e, 8, 9 and all of MIS 11 experienced more intense dissolution.

[29] Remarkably, MIS 11 stands out as the period of most pronounced dissolution because it is marked by low shell weights, the lowest % *G. ruber*, and the highest % fragments (more than twice the % fragments than in the other interglacial intervals). These data suggest MIS 11 was the most intense period of dissolution in the Caribbean over the past four glacial cycles. It should be noted that the dissolution peak recorded simultaneously by both the minimum of % *G. ruber* and the maximum of % fragment is concurrent with a mid-MIS 11 increase in *G. ruber* shell weight. We hypothesize that as dissolution increases, less massive shells fragment, leaving behind the more massive, dissolution resistant individuals. MIS 11 Mg/Ca ratios are more typical of glacial rather than interglacial temperatures, suggesting that dissolution has affected the minor element geochemistry in this part of our record. MIS 11 dissolution may have also increased the *G. ruber* $\delta^{18}\text{O}_\text{c}$ values, resulting in $\delta^{18}\text{O}_\text{c}$ values that are more enriched relative to younger interglacial intervals (MIS 1, 5e, 7 and 9) (Figure 3a) [Lohmann, 1995]. On the basis of these results, we conclude that the Mg/Ca ratios and $\delta^{18}\text{O}_\text{c}$ values from MIS 11 (375–423 kyr) do not represent a primary signal and therefore cannot be included in our subsequent discussion of Caribbean late Pleistocene SST evolution.

[30] We recognize that it is difficult to quantify the dissolution effect on the *G. ruber* Mg/Ca ratios from intervals with a fragmentation index between 10 and 20% (gray bars in Figure 3). At times, both shell weights and the % *G. ruber* decrease (MIS 5d, 7a, 7e, 8, and 9), suggesting that dissolution may have reduced the Mg concentration in these intervals. Broecker and Clark [2002] documented a dramatic dissolution event in the western Atlantic at the MIS 5e/5d transition, which they attribute to the invasion of corrosive Southern Ocean water farther northward into the western Atlantic. Similar invasions of southern waters into the Atlantic could also explain earlier dissolution cycles in our record. However, during MIS 7c, both shell weights and the % *G. ruber* increase, making it difficult to

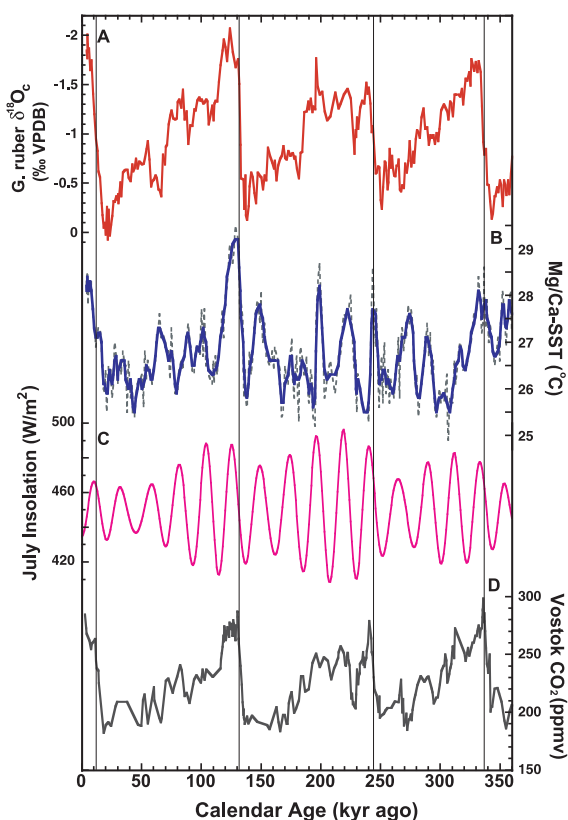


Figure 6. (a) ODP 999A *G. ruber* (white) $\delta^{18}\text{O}_e$ record and (b) Mg/Ca-SST record (fine line with weighted 3-point running mean) versus (c) July insolation variation at 12°N over the past 360 kyr. (d) Vostok CO_2 record [Petit *et al.*, 1999] on the methane-based timescale [Ruddiman and Raymo, 2003]. Vertical black lines indicate glacial termination events I–IV.

determine the impact of dissolution on intervals where the fragmentation index is between 10 and 20%. Recognizing these possible complications in discrete sections of ODP 999A, we have chosen to include all intermediate fragmentation intervals in our subsequent discussion of SST variability over the last 360 kyr.

8. Discussion

[31] Although total annual mean insolation is controlled by the 41 kyr obliquity periodicity [Loutre *et al.*, 2004] and almost exclusively dominates ice volume proxies, eccentricity-modulated precession, with a 23 and 100 kyr periodicity, controls seasonal insolation at a particular latitude [Raymo and Nisancioglu, 2003; Ruddiman and McIntyre, 1981]. Visual inspection of our Caribbean Mg/Ca-SST record shows a strong 23 and 100 kyr periodicity, but lacks a 41 kyr

frequency (Figure 6). As argued by Lea [2004] for Pacific SST variability, greenhouse forcing (GHF) due to changes in atmospheric CO_2 content modulates tropical SST at the 100 kyr frequency. The predominant 23 and 100 kyr periodicities in our Caribbean Mg/Ca-SST record therefore suggest that a combination of seasonal and greenhouse forcing, rather than ice volume dynamics, is the driver of our Caribbean Mg/Ca-SST record over the past 360 kyr. During interglacial periods when CO_2 levels were >250 ppm in the Vostok ice core record [Petit *et al.*, 1999], GHF may have amplified Caribbean warming (Figure 6). However, CO_2 amplification is an unlikely candidate to explain the glacial warming events that occur during MIS 4, 6, 8, and 10 because CO_2 is low at these times. The predominant 23 kyr frequency can best be explained if the Mg/Ca-SST record is biased toward a particular season.

[32] Spectral analysis (based on the Arand-package [Howell, 2001]) of the 360 kyr Mg/Ca-SST record shows strong spectral power at the $1/23$ kyr frequency (Figure 7), suggesting that the 999A Mg/Ca-SST is biased toward seasonal insolation variability. This conclusion is also supported by sediment flux data from the nearby Cariaco Basin, which confirms that the greatest seasonal flux of *G. ruber* (white) occurs from spring through late summer [Tedesco and Thunell, 2003]. Spectral analysis of the Mg/Ca-SST record also reveals a strong 100 kyr period and a weaker 29 kyr period. The 100 kyr cycle may be due to GHF that amplifies interglacial temperatures at this period. Several studies have also shown that precessional power is transferred to the eccentricity bands because climate is more responsive to insolation maxima than to minima [Pokras and Mix, 1987; Short *et al.*, 1991; Crowley, 1992; Harris and Mix, 1999], which may also contribute to the $1/100$ frequency in our SST record. Spectral power at the $1/29$ kyr frequency is commonly observed in $\delta^{18}\text{O}$ records and is thought to be a weak nonlinear climate response that results from an interaction between obliquity and eccentricity [Huybers and Wunsch, 2004; Lisiecki and Raymo, 2005].

[33] Visual comparison of our Mg/Ca-SST record with July insolation variability at 12°N shows that all but 1 (at 310 kyr) of 16 precessional cycles over the last 360 kyr correspond to SST oscillations (Figures 6b and 6c). Timing offsets between the Mg/Ca-SST record and seasonal insolation likely reflect age model variations imparted by tuning the

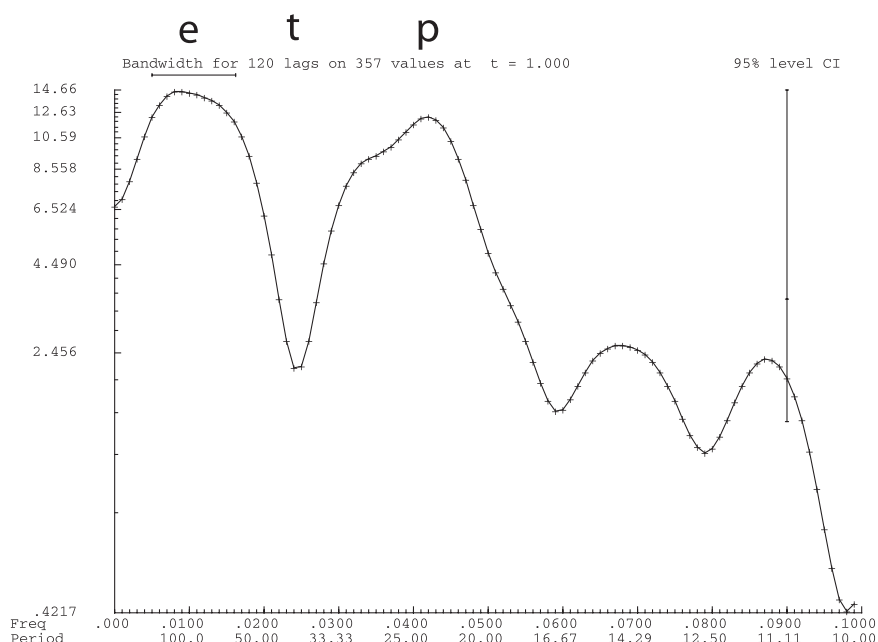


Figure 7. Amplitude spectra of the 999A Mg/Ca-SST record over the last 360 kyr, showing strong 23 kyr and 100 kyr power. Major earth orbital periods are indicated: *e* = eccentricity, *t* = tilt, *p* = precession.

$\delta^{18}\text{O}_c$ record to SPECMAP. Previous research showed the Caribbean experienced large salinity changes on glacial-interglacial timescales [Schmidt *et al.*, 2004], so tuning the ODP 999A planktonic foraminiferal $\delta^{18}\text{O}_c$ record to SPECMAP is particularly difficult at this site because the global ice-volume imprint on $\delta^{18}\text{O}_c$ can be offset by the regional hydrologic impact on surface salinity.

[34] On the basis of modeling results, Mix [1987] showed how the seasonal weighting of foraminiferal fluxes can affect the $\delta^{18}\text{O}_c$ record. If foraminiferal productivity is sensitive to temperature, the $\delta^{18}\text{O}_c$ value of the mean population will not record the mean annual temperature. Instead, foraminiferal populations will adjust their season (and/or depth) of maximum growth to choose water temperatures within their preferred range [Mix, 1987]. Assuming the seasons of maximum *G. ruber* flux were similar on glacial-interglacial timescales, we interpret the Mg/Ca-SST record from ODP 999A to represent the seasonally-weighted average SST from mid-spring through early fall. This interpretation is supported by the observation that the core top Mg/Ca-SST value is 0.5°C warmer than the modern annual mean SST for the study area, and more closely matches the average modern SST from May to October. Although August faunal SST reconstructions suggest that maximum glacial summer temperatures remained relatively constant in the Colombian Basin, the duration of the warm

season was likely shorter during glacial times and the seasonal temperature contrast was probably greater. As the duration of the warm season shortened and the seasonal contrast became more extreme, the *G. ruber* Mg/Ca-SST would have recorded cooler average temperatures despite the observation that August faunal SSTs remained nearly constant. Periods of maximum Mg/Ca-SST values (i.e., the early Holocene, MIS 5e, 7a, 7c, 7e and 9) likely represent periods when the Caribbean experienced longer periods of warm, summer-like temperatures when summer insolation and GHF were at a maximum.

[35] During the last 30 kyr, the Tobago Basin faunal summer month SST record (T_w) [Hüls and Zahn, 2000] is remarkably similar to our Colombian Basin Mg/Ca-SST record (Figure 5). The modern analog technique used by Hüls and Zahn [2000] estimates an average SST across the entire summer season, which may explain why their warm season temperatures are more similar to our seasonal *G. ruber*-based Mg/Ca-SST record than the warmest month (August) faunal SSTs estimates from 999A (Figure 4). However, from 30 to 50 kyr, the Mg/Ca-SSTs suggests the western Caribbean Colombian Basin was warmer than the Tobago Basin. In addition, the nearly constant faunal August SST record from 999A implies a steeper glacial summer SST gradient between these two sites. This east-west tropical Atlantic SST differ-

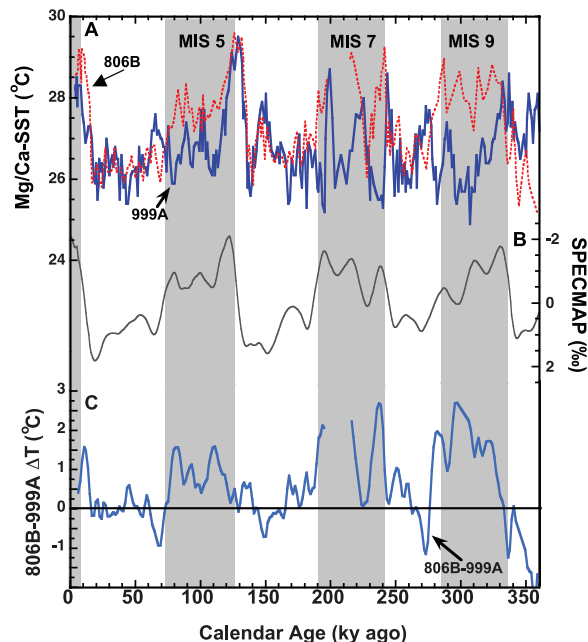


Figure 8. (a) Mg/Ca-SST records from ODP 999A (this study) (heavy blue line) and the western equatorial Pacific core ODP 806B (0°19'N; 159°22'E) (dashed red line) [Lea *et al.*, 2000]. Gray bars indicate interglacial periods. Caribbean SSTs are more similar to WEP values during glacial intervals. (b) Stacked SPECMAP [Bassinot *et al.*, 1994b] $\delta^{18}\text{O}$ record. (c) 806B - 999A SST gradient, calculated by interpolating the SST records at both sites to a constant interval of 1.5 kyr and smoothing the results with a weighted 3-point mean. Note that the SST gradient between the Caribbean and the WEP is reduced during glacials (i.e., closer to the zero line) but that the WEP experiences more warming during interglacials.

ence may be due to a southward shift in the glacial North Equatorial Current in the open Atlantic [Vink *et al.*, 2001], which would influence the Tobago Basin but not the Colombian Basin.

[36] Comparison of our long-term Caribbean Mg/Ca-SST record with a similar *G. ruber* Mg/Ca-SST record from the western equatorial Pacific (WEP) site ODP 806B (0°19'N, 159°22'E) [Lea *et al.*, 2000] shows that average SSTs in the WEP are higher than in the Caribbean during interglacial periods (Figure 8a). Although the SST gradient between sites 806B and 999A is greater during MIS 7 and 9 relative to the Holocene and MIS 5 (Figure 8c), this shift may be due in part to secular changes in carbonate preservation in the Caribbean prior to MIS 6. The largest SST differences between the WEP and the Caribbean occur during interglacial intervals where the fragmentation index

in ODP 999A is >10% (Figures 3e and 8c). Nevertheless, the east-west SST gradient between the Caribbean and the WEP collapses during glacial episodes when preservation is enhanced at both sites, reducing the interhemispheric SST gradient between these two locations. Similar to the Caribbean, maximum seasonal *G. ruber* productivity in the WEP occurs from late spring through fall [Kawahata *et al.*, 2002]. Figure 8c shows that the SST difference between 806B and 999A over the past 360 kyr closely tracks global ice-volume as recorded by SPECMAP. The correlation between SPECMAP ice volume and the SST difference between 806B and 999A suggests these two regions are linked through orbital-scale shifts in tropical atmospheric circulation.

[37] Modeling studies suggest that orbitally driven changes in the amount of seasonal solar insolation in the tropics influences ENSO variability, correlating warm periods (early Holocene and MIS 5e) with enhanced La Niña circulation and continental ice growth with stronger El Niño forcing [Bush and Philander, 1998; Cane and Clement, 1999; Cane, 1998; Clement and Cane, 1999; Clement *et al.*, 1999; Kukla *et al.*, 2002]. Recent geochemical proxy data from the tropical Pacific also suggest a link between North Atlantic stadials and El Niño-like events in the tropics [Koutavas *et al.*, 2002; Stott *et al.*, 2002; Visser *et al.*, 2003]. Not surprisingly, ENSO variability directly impacts climate in the tropical north Atlantic, resulting in reduced rainfall, warmer spring SSTs, and weaker trade winds in the western Tropical Atlantic during an El Niño event [Alexander and Scott, 2002; Alexander *et al.*, 2002; Giannini *et al.*, 2001; Poveda and Mesa, 1997]. Furthermore, the analysis of 40 years of data on the position of the ITCZ shows that its mean position is displaced southward during an El Niño phase, resulting in a rainfall deficit in Central America [Hastenrath, 2002]. Therefore a shift to a more El Niño-like glacial circulation mode should produce a warmer, drier Caribbean. Taken together with the recent report of increased glacial surface salinities in the Caribbean [Schmidt *et al.*, 2004], our Caribbean Mg/Ca-SST record of only 2.1°C of cooling at the LGM is consistent with both a southward migration of the glacial ITCZ and a glacial El Niño-like mode of tropical circulation.

[38] During a modern La Niña-state, spring trade winds in the tropical Atlantic are stronger, resulting in cooler Caribbean SSTs [Alexander and Scott, 2002; Alexander *et al.*, 2002; Enfield and Mayer,

1997; Saravanan and Chang, 2000] and warmer SSTs in the tropical western Pacific [Delcroix and McPhaden, 2002]. Therefore a shift to a more permanent La Niña-like interglacial climate state may explain the larger interglacial SST gradient between the Caribbean and the WEP.

9. Conclusions

[39] We evaluate how glacial-interglacial changes in preservation have impacted Mg/Ca ratios in planktonic foraminifera from the southwest Caribbean by measuring down-core changes in shell weight, the % *G. ruber*, and the degree of fragmentation. We show that it is possible to use these dissolution-sensitive records to identify intervals where dissolution has significantly reduced Mg/Ca ratios in *G. ruber* shells. Although we identify several brief periods of increased dissolution in our record, we show that MIS 11 stands out as the most intensive dissolution cycle in the Caribbean over the last 460 kyr. Therefore it is critical that future Mg/Ca paleothermometry studies fully consider how secular changes in preservation can affect Mg/Ca ratios in foraminiferal calcite.

[40] Our orbital-scale Mg/Ca-SST record from the Caribbean suggests that the last three glacial maximums were 2.1 to 2.5°C cooler than modern. A faunal August SST reconstruction from the same core shows only about 1°C cooling during glacial times, suggesting that maximum summer SSTs during glacial periods were not much cooler than the modern. Spectral analysis of the *G. ruber* Mg/Ca-SST record shows strong 23 and 100 kyr periods, which we interpret as indicating that the Mg/Ca-SST reconstruction is seasonally weighted toward warm months rather than reflecting the mean annual SST in the Colombian Basin. We suggest that summer insolation variability and GHF are the main drivers of SST variability in our Mg/Ca-SST record.

[41] Comparison of the 999A Mg/Ca-SST record over the past 360 kyr with a previously published record of Mg/Ca-SST change in the western tropical Pacific shows systematic changes in the east-west SST gradient on glacial-interglacial timescales. During glacial periods, the Caribbean-WEP SST gradient diminishes. A reduction in the SST difference between the Caribbean and western Pacific is consistent with a shift to a glacial El Niño-like mode of tropical circulation.

[42] Changes in the mean annual position of the ITCZ have a profound impact on climate in the Caribbean region. However, the position of the ITCZ is forced more by changes in the north-south SST gradient rather than by changes in mean tropical SST. A latitudinal SST anomaly of only 1°C from 15°N to 5°S in the tropical Atlantic can displace the ITCZ by hundreds of kilometers [Chiang et al., 2002], causing significant changes in tropical atmospheric circulation [Yin and Battisti, 2001]. Therefore additional studies are needed to quantify the magnitude and timing of SST change across a range of latitudes before we can determine how temporal shifts in the tropical hydrologic cycle are linked to global climate change.

Acknowledgments

[43] We thank the Ocean Drilling Program (ODP) for core samples. This material is based on work supported by a JOI-ODP Schlanger Ocean Drilling Fellowship to M.W.S. and by the National Science Foundation under Grant 0327060 to H.J.S. Additional funding was provided by the UC Davis Department of Geology Durrell Funds and by a UC Davis Humanities Fellowship to M.W.S. Laboratory assistance from D. Pak and numerous UC Davis undergraduate assistants and mass spectrometer operation by G. Paradis and D. Winter were critical to the success of this study. Elemental analyses were conducted in D. Lea's lab at UCSB. We also thank A. Droxler for providing a suite of his ODP 999A samples and D. Lea, A. Russell, and T. Hill for their valuable discussions and helpful comments and suggestions.

References

- Adelseck, C. G. (1978), Dissolution of deep-sea carbonate preliminary calibration of preservational and morphological aspects, *Deep Sea Res.*, 25, 1167–1185.
- Alexander, M., and J. Scott (2002), The influence of ENSO on air-sea interaction in the Atlantic, *Geophys. Res. Lett.*, 29(14), 1701, doi:10.1029/2001GL014347.
- Alexander, M. A., I. Blade, M. Newman, J. R. Lanzante, N. C. Lau, and J. D. Scott (2002), The atmospheric bridge: The influence of ENSO teleconnections on air-sea interaction over the global oceans, *J. Clim.*, 15, 2205–2231.
- Barker, S., and H. Elderfield (2002), Foraminiferal calcification response to glacial-interglacial changes in atmospheric CO₂, *Science*, 297, 833–836.
- Bassiot, F. C., L. Beaufort, E. Vincent, and L. Labeyrie (1994a), Coarse fraction fluctuations in pelagic carbonate sediments from the tropical Indian Ocean: A 1500 kyr record of carbonate dissolution, *Paleoceanography*, 9, 579–600.
- Bassiot, F. C., L. D. Labeyrie, E. Vincent, X. Quidelleur, N. J. Shackleton, and Y. Lancelot (1994b), The astronomical theory of climate and the age of the Brunhes-Matuyama magnetic reversal, *Earth Planet. Sci. Lett.*, 126, 91–108.

- Bé, A. W. H., and D. S. Tolderlund (1971), Distribution and ecology of living planktonic foraminifera in surface waters of the Atlantic and Indian Oceans, in *Micropaleontology of Oceans*, edited by B. M. Funnell and W. R. Riedel, pp. 105–149, Cambridge Univ. Press, New York.
- Bé, A. W. H., J. W. Morse, and S. M. Harrison (1975), Progressive dissolution and ultrastructural breakdown of planktonic foraminifera, *Spec. Publ. Cushman Found. Foraminiferal Res.*, 13, 27–55.
- Berger, W. H. (1967), Foraminiferal ooze: Solution at depth, *Science*, 156, 383–385.
- Berger, W. H. (1968), Shell production and preservation, Ph.D. thesis, Univ. of Calif. at San Diego, San Diego.
- Berger, W. H. (1970), Planktonic foraminifera: Selective solution and the lysocline, *Mar. Geol.*, 8, 111–138.
- Berger, W. H. (1982), Deglacial CO₂ buildup: Constraints on the coral-reef model, *Palaeogeogr. Palaeoclimatol. Palaeoecol.*, 40, 235–253.
- Berger, W. H., and D. J. W. Piper (1972), Planktonic foraminifera: Differential settling, dissolution and redeposition, *Limnol. Oceanogr.*, 17, 275–286.
- Bijma, J., H. J. Spero, and D. W. Lea (1999), Reassessing foraminiferal stable isotopes: Effects of seawater carbonate chemistry (experimental results), in *Use of Proxies in Paleoceanography: Examples From the South Atlantic*, edited by G. Fischer and G. Wefer, pp. 489–512, Springer, New York.
- Black, D. E., L. C. Peterson, J. T. Overpeck, A. Kaplan, M. N. Evans, and M. Kashgarian (1999), Eight centuries of North Atlantic ocean variability, *Science*, 286, 1709–1713.
- Bonneau, M., C. Vergnaudgrazzini, and W. H. Berger (1980), Stable isotope fractionation and differential dissolution in recent planktonic-foraminifera from Pacific box-cores, *Oceanol. Acta*, 3, 377–382.
- Boyle, E. A., and L. D. Keigwin (1987), North Atlantic thermohaline circulation during the last 20,000 years linked to high latitude surface temperature, *Nature*, 330, 35–40.
- Broecker, W., and E. Clark (2001), An evaluation of Lohmann's foraminifera weight dissolution index, *Paleoceanography*, 16, 531–534.
- Broecker, W. S., and E. Clark (2002), A major dissolution event at the close of MIS 5e in the western equatorial Atlantic, *Geochem. Geophys. Geosyst.*, 3(2), 1009, doi:10.1029/2001GC000210.
- Brown, S., and H. Elderfield (1996), Variations in Mg/Ca and Sr/Ca ratios of planktonic foraminifera caused by postdepositional dissolution: Evidence of shallow Mg-dependent dissolution, *Paleoceanography*, 11, 543–551.
- Bush, A. G., and S. H. Philander (1998), The role of ocean-atmosphere interactions in tropical cooling during the last glacial maximum, *Science*, 279, 1341–1344.
- Cane, M. A. (1998), A role for the tropical Pacific, *Science*, 282, 59–61.
- Cane, M., and A. C. Clement (1999), A role for the tropical Pacific coupled ocean-atmosphere system on Milankovitch and millennial timescales. Part II: Global impacts, in *Mechanisms of Global Climate Change at Millennial Time Scales*, *Geophys. Monogr. Ser.*, vol. 112, edited by P. U. Clark, R. S. Webb, and L. D. Keigwin, pp. 373–384, AGU, Washington, D. C.
- Chappell, J., A. Omura, T. Esat, M. T. McCulloch, J. Pandolfi, Y. Ota, and B. Pillans (1996), Reconciliation of late Quaternary sea levels derived from coral terraces at Huon Peninsula with deep sea oxygen isotope records, *Earth Planet. Sci. Lett.*, 141, 227–236.
- Chiang, J. C. H., Y. Kushnir, and A. Giannini (2002), Deconstructing Atlantic Intertropical Convergence Zone variability: Influence of the local cross-equatorial sea surface temperature gradient and remote forcing from the eastern equatorial Pacific, *J. Geophys. Res.*, 107(D1), 4004, doi:10.1029/2000JD000307.
- Clement, A. C., and M. Cane (1999), A role for the Tropical Pacific coupled ocean-atmosphere system on Milankovitch and millennial timescales. Part I: A modeling study of Tropical Pacific variability, in *Mechanisms of Global Climate Change at Millennial Time Scales*, *Geophys. Monogr. Ser.*, vol. 112, edited by P. U. Clark, R. S. Webb, and L. D. Keigwin, pp. 363–372, AGU, Washington, D. C.
- Clement, A. C., R. Seager, and M. A. Cane (1999), Orbital controls on the El Niño/southern oscillation and the tropical climate, *Paleoceanography*, 14, 441–456.
- Conkright, M. E., S. Levitus, T. O'Brien, T. P. Boyer, J. Antonov, and C. Stephens (2002), *World Ocean Atlas 2001: Objective Analyses, Data Statistics, and Figures* [CD-ROM], 17 pp., Natl. Oceanogr. Data Cent., Silver Spring, Md.
- Coulbourn, W. T., F. L. Parker, and W. H. Berger (1980), Faunal and solution patterns of planktonic foraminifera in surface sediments of the North Pacific, *Mar. Micropaleontol.*, 5, 329–399.
- Crowley, T. J. (1992), North Atlantic Deep Water cools the southern hemisphere, *Paleoceanography*, 7, 489–497.
- Dekens, P. S., D. W. Lea, D. K. Pak, and H. J. Spero (2002), Core top calibration of Mg/Ca in tropical foraminifera: Refining paleotemperature estimation, *Geochem. Geophys. Geosyst.*, 3(4), 1022, doi:10.1029/2001GC000200.
- Delcroix, T., and M. McPhaden (2002), Interannual sea surface salinity and temperature changes in the western Pacific warm pool during 1992–2000, *J. Geophys. Res.*, 107(C12), 8002, doi:10.1029/2001JC000862.
- de Villiers, S. (2004), Optimum growth conditions as opposed to calcite saturation as control on the calcification rate and shell-weight of marine foraminifera, *Mar. Biol.*, 144, 45–49.
- Emiliani, C. (1966), Paleotemperature analysis of Caribbean cores P6304-8 and P6304-9 and a generalized temperature curve for the past 425,000 years, *J. Geol.*, 74, 109–123.
- Enfield, D. B., and D. A. Mayer (1997), Tropical Atlantic sea surface temperature variability and its relation to El Niño Southern Oscillation, *J. Geophys. Res.*, 102, 929–945.
- Giannini, A., J. C. H. Chiang, M. A. Cane, Y. Kushnir, and R. Seager (2001), The ENSO teleconnection to the tropical Atlantic Ocean: Contributions of the remote and local SSTs to rainfall variability in the tropical Americas, *J. Clim.*, 14, 4530–4544.
- Harris, S. E., and A. C. Mix (1999), Pleistocene precipitation balance in the Amazon Basin recorded in deep sea sediments, *Quat. Res.*, 51, 14–26.
- Hastenrath, S. (2002), The intertropical convergence zone of the eastern Pacific revisited, *Int. J. Climatol.*, 22, 347–356.
- Hastings, D. W., A. D. Russell, and S. R. Emerson (1998), Foraminiferal magnesium in *Globigerinoides sacculifer* as a paleotemperature proxy, *Paleoceanography*, 13, 161–169.
- Honjo, S., and J. Erez (1978), Dissolution rates of calcium carbonate in the deep ocean: An in-situ experiment in the North Atlantic Ocean, *Earth Planet. Sci. Lett.*, 40, 287–300.
- Howard, W. R., and W. L. Prell (1994), Late Quaternary CaCO₃ production and preservation in the Southern Ocean: Implications for oceanic and atmospheric carbon cycling, *Paleoceanography*, 9, 453–482.
- Howell, P. (2001), ARAND time series and spectral analysis package for the Macintosh, Brown Univ., in *IGBP PAGES/World Data Center for Paleoclimatology Data Contribution Series #2001–044*, NOAA/NGDC Paleoclimatol. Program, Boulder, Colo.

- Hughen, K. A., J. T. Overpeck, L. C. Peterson, and S. E. Trumbore (1996), Rapid climate changes in the tropical Atlantic region during the last deglaciation, *Nature*, **380**, 51–54.
- Hughen, K. A., J. T. Overpeck, S. J. Lehman, M. Kashgarian, J. Southon, L. C. Peterson, R. Alley, and D. M. Sigman (1998), Deglacial changes in ocean circulation from an extended radiocarbon calibration, *Nature*, **391**, 65–68.
- Hüls, M., and R. Zahn (2000), Millennial-scale sea surface temperature variability in the western tropical North Atlantic from planktonic foraminiferal census counts, *Paleoceanography*, **15**, 659–678.
- Huybers, P., and C. Wunsch (2004), A depth-derived Pleistocene age model: Uncertainty estimates, sedimentation variability, and nonlinear climate change, *Paleoceanography*, **19**, PA1028, doi:10.1029/2002PA000857.
- Imbrie, J., and N. G. Kipp (1971), A new micropaleontological method for paleoclimatology: Application to a late Pleistocene Caribbean core, in *The Late Cenozoic Glacial Ages*, edited by K. K. Turekian, pp. 71–181, Yale Univ. Press, New Haven, Conn.
- Johns, W. E., T. L. Townsend, D. M. Fratantoni, and W. D. Wilson (2002), On the Atlantic inflow to the Caribbean Sea, *Deep Sea Res., Part I*, **49**, 211–243.
- Johnson, D. A., M. Ledbetter, and L. H. Burckle (1977), Vema Channel paleoceanography: Pleistocene dissolution cycles and episodic bottom water flow, *Mar. Geol.*, **23**, 1–33.
- Kameo, K., M. C. Shearer, A. W. Droxler, I. Mita, R. Watanabe, and T. Sato (2004), Glacial-interglacial surface water variations in the Caribbean Sea during the last 300 ky based on calcareous nannofossil analysis, *Paleogeogr. Paleoclimatol. Paleoeconol.*, **212**, 65–76.
- Kawahata, H., A. Nishimura, and M. K. Gagan (2002), Seasonal change in foraminiferal production in the western equatorial Pacific warm pool: Evidence from sediment trap experiments, *Deep Sea Res., Part II*, **49**, 2783–2800.
- Kennett, J. P., and M. S. Srinivasan (1983), *Neogene Planktonic Foraminifera*, 265 pp., Hutchinson Ross, Stroudsburg, Pa.
- Koutavas, A., J. Lynch-Stieglitz, T. M. Marchitto, Jr., and J. P. Sachs (2002), El Niño-like pattern in Ice Age tropical Pacific sea surface temperature, *Science*, **297**, 226–229.
- Kukla, G., A. C. Clement, M. Cane, J. Gavin, and S. Zebiak (2002), Last interglacial and early glacial ENSO, *Quat. Res.*, **58**, 27–31.
- Le, J., and N. D. Shackleton (1992), Carbonate dissolution fluctuations in the western equatorial Pacific during the late Quaternary, *Paleoceanography*, **7**, 21–42.
- Lea, D. W. (2004), The 100,000-yr cycle in tropical SST, greenhouse forcing, and climate sensitivity, *J. Clim.*, **17**, 2170–2179.
- Lea, D. W., and P. A. Martin (1996), A rapid mass spectrometric method for the simultaneous analysis of barium, cadmium, and strontium in foraminifera shells, *Geochim. Cosmochim. Acta*, **60**, 3143–3149.
- Lea, D. W., D. K. Pak, and H. J. Spero (2000), Climate impact of late Quaternary equatorial Pacific sea surface temperature variations, *Science*, **289**, 1719–1724.
- Lea, D. W., D. K. Pak, L. C. Peterson, and K. A. Hughen (2003), Synchronicity of tropical high latitude Atlantic temperatures over the last glacial termination, *Science*, **301**, 1361–1364.
- Lin, H. L., L. C. Peterson, J. T. Overpeck, S. E. Trumbore, and D. W. Murray (1997), Late Quaternary climate change from $\delta^{18}\text{O}$ records of multiple species of planktonic foraminifera: High-resolution records from the anoxic Cariaco Basin, Venezuela, *Paleoceanography*, **12**, 415–427.
- Lisiecki, L. E., and M. E. Raymo (2005), A Pliocene-Pleistocene stack of 57 globally distributed benthic $\delta^{18}\text{O}$ records, *Paleoceanography*, **20**, PA1003, doi:10.1029/2004PA001071.
- Lohmann, G. P. (1995), A model for variation in the chemistry of planktonic foraminifera due to secondary calcification and selective dissolution, *Paleoceanography*, **10**, 445–457.
- Loutre, M. F., D. Paillard, F. Vimeux, and E. Cortijo (2004), Does mean annual insolation have the potential to change the climate?, *Earth Planet. Sci. Lett.*, **221**, 1–14.
- Manabe, S., and R. J. Stouffer (1997), Coupled ocean-atmosphere model response to freshwater input: Comparison to Younger Dryas event, *Paleoceanography*, **12**, 321–336.
- Mashiotta, T. A., D. W. Lea, and H. J. Spero (1999), Glacial-interglacial changes in Subantarctic sea surface temperature and $\delta^{18}\text{O}$ -water using foraminiferal Mg, *Earth Planet. Sci. Lett.*, **170**, 417–432.
- Mix, A. (1987), The oxygen-isotope record of glaciation, in *North America and Adjacent Ocean During the Last Deglaciation*, edited by W. F. Ruddiman and H. E. Wright, Geol. Soc. Am., Boulder, Colo.
- Mutti, M. (2000), Bulk $\delta^{18}\text{O}$ and $\delta^{13}\text{C}$ records from site 999, Colombian Basin, and site 1000, Nicaraguan (latest Oligocene to middle Miocene): Diagenesis, link to sediment parameters, and paleoceanography, *Proc. Ocean Drill. Program Sci. Results*, **165**, 275–283.
- Oppo, D. W., and R. G. Fairbanks (1987), Variability in the deep and intermediate water circulation of the Atlantic Ocean during the past 25,000 years: Northern hemisphere modulation of the southern ocean, *Earth Planet. Sci. Lett.*, **86**, 1–15.
- Oppo, D. W., and S. J. Lehman (1993), Mid-depth circulation of the subpolar north Atlantic during the last glacial maximum, *Science*, **259**, 1148–1152.
- Pedersen, T. F., and N. B. Price (1982), The geochemistry of manganese carbonate in Panama Basin sediments, *Geochim. Cosmochim. Acta*, **46**, 59–68.
- Pena, L. D., I. Cacho, E. Calvo, S. Eggins, C. Pelejero, and N. J. Shackleton (2004), Rapid temperature oscillations in the eastern equatorial Pacific during the last deglaciation and Holocene periods, paper presented at International Conference on Paleoceanography VIII, EPOC Paleoceanogr. Group, Univ. Bordeaux I, Biarritz, France.
- Pena, L. D., E. Calvo, I. Cacho, S. Eggins, and C. Pelejero (2005), Identification and removal of Mn-Mg-rich contaminant phases on foraminiferal tests: Implications for Mg/Ca past temperature reconstructions, *Geochem. Geophys. Geosyst.*, **6**, Q09P02, doi:10.1029/2005GC000930.
- Peterson, L. C., and G. H. Haug (2006), Variability in the mean latitude of the Atlantic ITCZ as recorded by riverine input of sediments to the Cariaco Basin (Venezuela), *Paleogeogr. Paleoclimatol. Paleoeconol.*, in press.
- Peterson, L. C., and W. L. Prell (1985), Carbonate dissolution in recent sediments of the eastern equatorial Indian Ocean: Preservation patterns and carbonate loss above the lysocline, *Mar. Geol.*, **64**, 259–290.
- Peterson, L. C., G. H. Haug, K. A. Hughen, and U. Rohl (2000), Rapid changes in the hydrologic cycle of the Tropical Atlantic during the last Glacial, *Science*, **290**, 1947–1951.
- Petit, J. R., et al. (1999), Climate and atmospheric history of the last 420,000 years from the Vostok ice core, Antarctica, *Nature*, **399**, 429–436.

- Pflaumann, U., J. Duprat, C. Pujol, and J. Labeyrie (1996), SIMMAX: A modern analog technique to deduce Atlantic sea surface temperatures from planktonic foraminifera in deep-sea sediments, *Paleoceanography*, *11*, 15–35.
- Pflaumann, U., et al. (2003), Glacial North Atlantic: Sea-surface conditions reconstructed by GLAMAP 2000, *Paleoceanography*, *18*(3), 1065, doi:10.1029/2002PA000774.
- Philander, S. G. H., D. Gu, D. Halpern, G. Lambert, N. C. Lau, T. Li, and R. C. Pacanowski (1996), Why the ITCZ is mostly north of the equator, *J. Clim.*, *9*, 2958–2972.
- Pierrehumbert, R. T. (1995), Thermostats, radiator fins, and the local runaway greenhouse, *J. Atmos. Sci.*, *52*, 1784–1806.
- Pokras, E. M., and A. C. Mix (1987), Earth's precession cycle and Quaternary climatic change in tropical Africa, *Nature*, *326*, 486–487.
- Poveda, G., and O. J. Mesa (1997), Feedbacks between hydrological processes in tropical South America and large-scale ocean-atmospheric phenomena, *J. Clim.*, *10*, 2690–2702.
- Poveda, G., P. R. Waylen, and R. S. Pulwarty (2006), Annual and interannual variability of the present climate in northern South America and southern Mesoamerica, *Paleogeogr. Paleoclimatol. Paleoecol.*, in press.
- Prell, W., J. V. Gardner, A. W. Be, and J. D. Hays (1976), Equatorial Atlantic and Caribbean foraminiferal assemblages, temperatures, and circulation: Interglacial and glacial comparisons, *Mem. Geol. Soc. Am.*, *145*, 247–266.
- Raymo, M. E., and K. Nisancioglu (2003), The 41 kyr world: Milankovitch's other unsolved mystery, *Paleoceanography*, *18*(1), 1011, doi:10.1029/2002PA000791.
- Roemmich, D. H., and C. Wunsch (1985), Two transatlantic sections: Meridional circulation and heat flux in the subtropical North Atlantic Ocean, *Deep Sea Res., Part I*, *32*, 619–664.
- Rosenthal, Y., and G. P. Lohmann (2002), Accurate estimation of sea surface temperatures using dissolution-corrected calibrations for Mg/Ca paleothermometry, *Paleoceanography*, *17*(3), 1044, doi:10.1029/2001PA000749.
- Rosenthal, Y., D. W. Oppo, and B. K. Linsley (2003), The amplitude and phasing of climate change during the last deglaciation in the Sulu Sea, western equatorial Pacific, *Geophys. Res. Lett.*, *30*(8), 1428, doi:10.1029/2002GL016612.
- Ruddiman, W. F., and A. McIntyre (1981), Oceanic mechanisms for amplification of the 23,000-year ice-volume cycle, *Science*, *212*, 617–627.
- Ruddiman, W. F., and M. E. Raymo (2003), A methane-based time scale for Vostok ice, *Quat. Sci. Rev.*, *22*, 141–155.
- Ruhlemann, C., S. Mulitza, P. J. Muller, G. Wefer, and R. Zahn (1999), Warming of the tropical Atlantic Ocean and slow-down of thermohaline circulation during the last deglaciation, *Nature*, *402*, 511–514.
- Saravanan, R., and P. Chang (2000), Interaction between tropical Atlantic variability and El Niño-Southern Oscillation, *J. Clim.*, *13*, 2177–2194.
- Schiffelbein, P., and S. Hills (1984), Direct assessment of stable isotope variability in planktonic-foraminifera populations, *Paleogeogr. Paleoclimatol. Paleoecol.*, *48*, 197–213.
- Schiller, A., U. Mikolajewicz, and R. Voss (1997), The stability of North Atlantic thermohaline circulation in a coupled ocean-atmosphere general circulation model, *Clim. Dyn.*, *13*, 325–347.
- Schmidt, M. W., H. J. Spero, and D. W. Lea (2004), Links between salinity variation in the Caribbean and North Atlantic thermohaline circulation, *Nature*, *428*, 160–163.
- Seidov, D., and M. Maslin (2001), Atlantic Ocean heat piracy and the bipolar climate see-saw during Heinrich and Dansgaard-Oeschger events, *J. Quat. Sci.*, *16*, 321–328.
- Short, D. A., J. G. Mengel, T. J. Crowley, W. T. Hyde, and G. R. North (1991), Filtering of Milankovitch cycles by Earth's geography, *Quat. Res.*, *35*, 157–173.
- Spero, H. J. (1992), Do planktic foraminifera accurately record shifts in the carbon isotopic composition of seawater ΣCO_2 ?, *Mar. Micropaleontol.*, *19*, 275–285.
- Spero, H. J., K. M. Mielke, E. M. Kalve, D. W. Lea, and D. K. Pak (2003), Multispecies approach to reconstructing eastern equatorial Pacific thermocline hydrography during the past 360 kyr, *Paleoceanography*, *18*(1), 1022, doi:10.1029/2002PA000814.
- Stidd, C. K. (1967), The use of eigenvectors for climate estimates, *J. Appl. Meteorol.*, *6*, 255–264.
- Stott, L. D., C. Poulsen, S. Lund, and R. Thunell (2002), Super ENSO and global climate oscillations at millennial time scales, *Science*, *297*, 222–226.
- Stuiver, M., and P. J. Reimer (1993), Extended ^{14}C database and revised CALIB radiocarbon calibration program, *Radiocarbon*, *35*, 215–230.
- Tedesco, K. A., and R. C. Thunell (2003), Seasonal and interannual variations in planktonic foraminiferal flux and assemblage composition in the Cariaco Basin, Venezuela, *J. Foraminiferal Res.*, *33*, 192–210.
- Vellinga, M., and R. A. Wood (2002), Global climatic impacts of a collapse of the Atlantic thermohaline circulation, *Clim. Change*, *54*, 251–267.
- Vink, A., C. Ruhlemann, K. A. F. Zonneveld, S. Mulitza, M. Hüls, and H. Willems (2001), Shifts in the position of the north equatorial current and rapid productivity changes in the western tropical Atlantic during the last glacial, *Paleoceanography*, *16*, 479–490.
- Visser, K., R. Thunell, and L. D. Stott (2003), Magnitude and timing of temperature change in the Indo-Pacific warm pool during deglaciation, *Nature*, *421*, 152–155.
- Wolff, T., S. Mulitza, H. W. Arz, J. Patzold, and G. Wefer (1998), Oxygen isotopes versus CLIMAP (18 ka) temperatures: A comparison from the tropical Atlantic, *Geology*, *26*, 675–678.
- Yarincik, K. M., R. W. Murray, and L. C. Peterson (2000), Climatically sensitive eolian and hemipelagic deposition in the Cariaco Basin, Venezuela, over the past 578,000 years: Results from Al/Ti and K/Al, *Paleoceanography*, *15*, 210–228.
- Yin, J. H., and D. S. Battisti (2001), The importance of tropical sea surface temperature patterns in simulations of last glacial maximum climate, *J. Clim.*, *14*, 565–581.